New Journal of Physics
The open–access journal for physics

Sr_2RhO_4: a new, clean correlated electron metal

R S Perry[1], F Baumberger[1,2], L Balicas[3], N Kikugawa[1], N J C Ingle[2], A Rost[1], J F Mercure[1], Y Maeno[4,5], Z X Shen[2] and A P Mackenzie[1]

[1] School of Physics and Astronomy and Scottish Universities Physics Alliance, University of St. Andrews, St. Andrews KY16 9SS, UK
[2] Departments of Applied Physics, Physics, and Stanford Synchrotron Radiation Laboratory, Stanford University, Stanford, CA 94305, USA
[3] National High Magnetic Field Laboratory, 1800 E. Paul Dirac Dr., Tallahassee, 32310, USA
[4] Department of Physics, Kyoto University, Kyoto 606-8502, Japan
[5] Kyoto University International Innovation Center, Kyoto 606-8501, Japan
E-mail: rsp1@st-and.ac.uk and apm9@st-and.ac.uk

New Journal of Physics **8** (2006) 175
Received 3 May 2006
Published 1 September 2006
Online at http://www.njp.org/
doi:10.1088/1367-2630/8/9/175

Abstract. We report the image furnace growth of single crystals of a novel correlated electron metal, the rhodate Sr_2RhO_4. Suitable annealing treatments result in residual resistivity ratios in excess of 100. Bulk specific heat and magnetic susceptibility have been measured, and both the de Haas-van Alphen and Shubnikov-de Haas effects are observable in the best crystals. The quasi-two-dimensional electronic structure has also enabled a comprehensive study of the electronic structure by angle-resolved photoelectron spectroscopy. The implications of our combined spectroscopic results are discussed.

PII: S1367-2630(06)23714-5

Contents

1. Introduction

From the most general perspective, the term 'correlated electrons' refers to electrons in materials in which their kinetic, or 'delocalization' energy is in close competition with a potential energy which provides a drive for localization. In practice, obtaining these conditions usually means working with 'narrow band' materials in which the periodic potential from the ion cores is relatively strong. These conditions are best satisfied in materials whose conduction electrons delocalize from either d or f shells of the constituent atoms. High temperature superconductors [1] and colossal magnetoresistive manganites [2] involve 3d transition metal electrons, while f electrons are crucial in many heavy fermion systems [3]. Fascinating physics results in each of these systems, but there are some drawbacks. In most 3d transition metal oxides, the potential energy term (encapsulated in Hubbard model language as the on-site repulsion U) dominates the kinetic energy (the Hubbard model t), resulting in Mott–Hubbard insulators in which special material tricks must be employed to produce metallic conductivity. The most prominent of these, chemical doping, has the disadvantage of introducing fairly high levels of disorder. Doping is not usually needed to metallize 5f systems, but the high atomic numbers of the atoms providing the 5f electrons mean that large spin–orbit coupling always plays a significant role in the resultant physics.

Transition metal oxides based on 4d electrons sit between these two limits and provide an excellent opportunity to obtain complementary insights in the field. The most widely studied family is the ruthenates. The fact that they exist very close to a critical value of U/t is demonstrated by the wide range of physical properties that can be observed in them: small structural changes can send them all the way from correlated electron insulators to high conductivity metals which make transitions to subtle superconducting and magnetic ground states [4]–[6]. A key feature of the metals in the ruthenate series is the low levels of disorder with which they can be prepared. Since materials such as $SrRuO_3$, Sr_2RuO_4, $Sr_3Ru_2O_7$, $Sr_4Ru_3O_{10}$ and $Ca_3Ru_2O_7$ are metallic

in their stoichiometric form [5]–[11], the task of purifying them has become one of modern 'oxide metallurgy', performed over the past decade by several groups world-wide. The purest crystals are those of Sr_2RuO_4, in which remarkable residual resistivities of less than 70 nΩ cm, corresponding to mean free paths of several μm, have been achieved [12]. Impressive advances have also been made in the other materials. Although single crystals are more difficult to grow because of less favourable chemical phase diagrams, mean free paths in excess of 1000 Å can be attained [6]–[10].

One of the first tangible advantages of producing oxide metals with long mean free paths is that it enables the observation of quantum oscillations (often referred to as the de Haas-van Alphen or dHvA effect), which represent a direct and detailed observation of the low energy fermionic excitations of the metallic state. Observations such as these are still sufficiently rare in correlated electron systems that they are of considerable interest in their own right, but they become crucial if the high levels of purity which enabled them also facilitate the formation of an anisotropic collective state such as the superconductivity of Sr_2RuO_4. In such materials one has knowledge not just of exotic collective behaviour but also of the metallic quasiparticles from which the condensate formed.

There is, therefore, considerable motivation to find other correlated oxide metals based on 4d electrons. One route to this would be to extend the set of available ruthenates, but this is a somewhat restricted approach, because the underlying electronic structures of all ruthenates are all very similar. In the structurally simplest material, Sr_2RuO_4, three bands based on the t_{2g} orbitals of Ru cross the Fermi level, and since Ru is in its 4+ oxidation state, they accommodate four electrons. Many of the other materials have more complicated Fermi surfaces because of band folding due to symmetry-lowering structural distortions, but the basic bands that undergo the folding are all similar to those of Sr_2RuO_4. In the work reported here, we have taken another tack, by replacing ruthenium by rhodium. Rh^{4+} has five electrons in the t_{2g} orbitals, so in purifying Sr_2RhO_4 we make a significant change to the basic electronic structure near the Fermi level.

2. Experiments and bulk properties

2.1. Crystal growth, annealing and characterization

Single crystals of Sr_2RhO_4 were grown using a flux feeding floating zone technique using an infrared image furnace Canon Machinery SCI-MDH-11020 at St. Andrews, UK and NEC Machinery SC-K15HD-HP at Kyoto, Japan [13]. This method uses excess rhodium as both a self-flux and to compensate for the high vapour pressure of rhodium oxide. Initially, $SrCO_3$ (Sigma Aldrich, 99.99%) and Rh_2O_3 (Rare Metallic, 99.9%) were ground together using mortar and pestle in the ratio $Sr_2Rh_xO_y$ where $x = 1.15$. The powders were then pressed in pellets and calcined under flowing oxygen at 1400°C for 24 h. A high temperature and flowing oxygen were necessary to aid the oxidation of Rh^{3+} to Rh^{4+}. Also, at low oxygen stoichiometry ($y < 3.96$) the Sr_2RhO_4 phase is unstable to the Sr_4RhO_6 phase [14]. The resultant powder was around 2 : 1 Sr_2RhO_4 phase and Sr_4RhO_6 phase. Subsequently re-grindings and sintering could improve this ratio but it was found to have very little improvement on the Sr_2RhO_4 crystals after growth in the image furnace. The polycrystalline material was then re-ground and pressed into a rod of around 5 mm diameter using a hydrostatic press, sintered at 1450°C for 2 h under O_2 and set into the image furnace. Care was taken to ensure that Sr_2RhO_4 bedding material was used during sintering to avoid contamination from the alumina crucible. The growth conditions inside

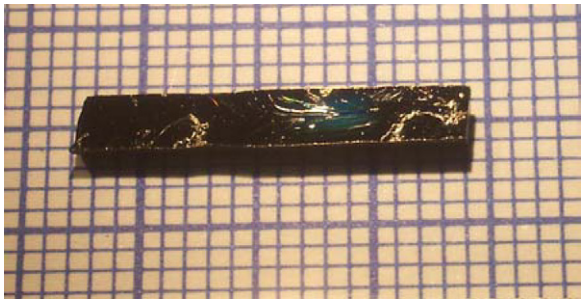

Figure 1. An image-furnace grown single crystal of Sr_2RhO_4. The small squares on the graph paper are millimetres, so this piece is over 1.5 cm long.

the image furnace were 100% O_2 at 10 bar pressure and growth speed of 10 mm h^{-1}. Typically, around 4–5% of the material used from the rod was lost due to evaporation. Successful crystal growth runs were made at both Kyoto and St. Andrews although the later runs at St. Andrews produced better quality crystals. We were able to grow single crystals of mass up to 0.5 g and confirm their phase purity using powder x-ray diffraction. A typical crystal piece is shown in figure 1.

The quality of the single crystals was confirmed using resistivity measurements to determine the temperature independent or elastic, impurity scattering. The crystals were cut into bar shaped pieces, of typical dimension $1 \times 0.2\,\mathrm{mm}^2$ in the crystallographic *ab* plane and 50 μm along the *c*-axis. Contacts were fixed to the crystal using gold wire and high temperature curing silver paste (Dupont 6838). The silver paste was annealed at 470°C under O_2.

As-grown crystals were actually poorly metallic, with room temperature resistivities of around 2 mΩ cm and a weakly negative $\partial\rho/\partial T$. To improve the quality, the crystals were annealed under O_2 at 1150°C for 2 weeks. The crystals were significantly improved and residual resistivity ratios (RRR) of between 40 and 120 were achieved. Figure 2 shows the temperature dependence of ρ for three of the crystals, post-annealing. The optimum value of x in the starting composition $Sr_2Rh_xO_y$ was found to be $x = 1.15$. Other values of x were tried but no systematic improvement in the RRR was noted. The effect of the annealing on oxygen stoichiometry was investigated by subjecting as-grown crystals to thermogravimetric analysis. On heating between room temperature and 900°C the crystals gained $\sim$0.5% by mass of oxygen, corresponding to $\sim$0.1 oxygen per formula unit. The measurements gave no reliable information on the absolute oxygen content, however, so we are unable to know for certain whether this brought initially oxygen-poor crystals up to stoichiometry or whether the annealed crystals are slightly hole-doped.

2.2. Electrical transport

An intriguing feature of the data shown in figure 2 is the temperature dependence. Between 50 and 250 K the resistivity has a quadratic temperature dependence to quite high accuracy. Below 50 K, however, we observe a flatter dependence than this, correponding to a temperature exponent of approximately 2.4. This is in interesting contrast to the behaviour seen in all the ruthenates that we have studied, in which the maximum power observed in zero applied magnetic field is 2 at the lowest temperatures, crossing over to less than 2 at temperatures which are generally less than 50 K [16]. We offer no explanation for the current observation on Sr_2RhO_4, which has been

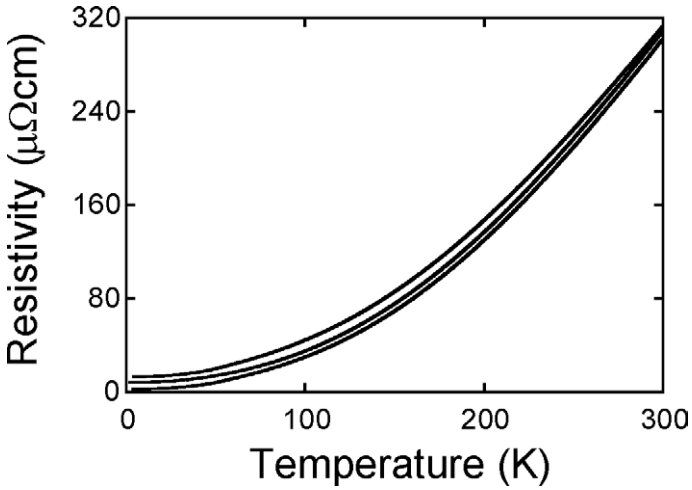

Figure 2. The *ab* plane resistivity of three annealed single crystals of Sr_2RhO_4. Standard geometrical uncertainties (crystal thickness, contact size, etc) limit the absolute accuracy of the resistivity measurement on any one crystal to 10–15%, so a higher accuracy room temperature value of $298 \pm 11\ \mu\Omega$ cm was deduced by taking the mean and its error from measurements on 15 separate high RRR crystals, in a procedure similar to that discussed in [15]. To produce the data shown here, each trace was first set to 300 $\mu\Omega$ cm at 300 K, and the RRR used to calculate the low temperature resistivity values, which are 13.0, 8.2 and 2.6 $\mu\Omega$ cm respectively. This was then assumed to be a temperature-independent constant contribution to the resistivity of that crystal.

repeated, post annealing, on all crystals that we have studied. Preliminary measurements of the *c*-axis resistivity show it to be metallic at low temperatures, with typical values of several mΩ cm. This large resistive anisotropy confirms the strongly two-dimensional nature of the electronic structure.

2.3. Specific heat

One of the most important bulk measurements to perform on a new correlated electron metal is the electronic specific heat C_p, which measures the sum of all the low energy excitations. The electronic specific heat coefficient, γ, gives the quasiparticle density of states averaged over the whole Fermi surface. For comparison of the physics of the two materials, and as a careful check on the calibration of the instrument, we performed back-to-back measurements (Quantum Design PPMS) of C_p on similar sized crystals of Sr_2RhO_4 and Sr_2RuO_4, for which γ is well known [5, 17]. The results are presented in figure 3.

2.4. Magnetic susceptibility

We have carried out preliminary magnetic susceptibility (χ) measurements on our crystals in a Quantum Design MPMS SQUID magnetometer, with results as shown in figure 4. Above 50 K, χ is very mildly temperature dependent and almost isotropic, in common with previous findings on, for example, Sr_2RuO_4. As argued for that material, it seems likely that this susceptibility is

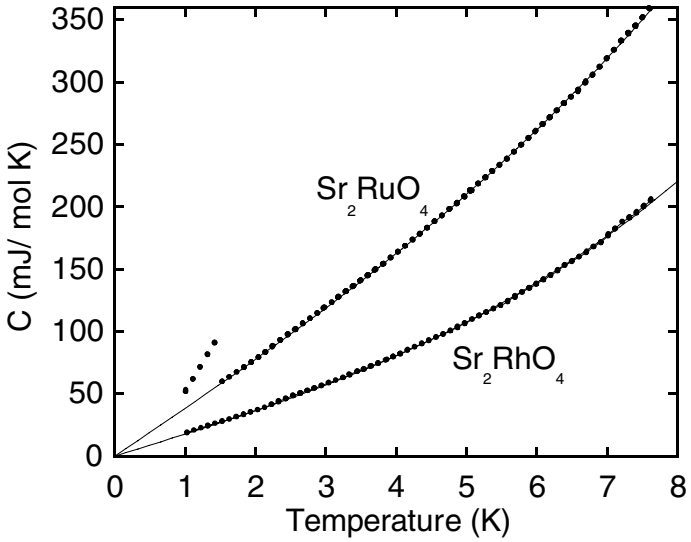

Figure 3. Specific heat at constant pressure, C_p, of Sr_2RuO_4 and Sr_2RhO_4. The dominance of the linear electronic term is clearly seen for both compounds below approximately 5 K, and the superconducting transition at 1.5 K is well resolved in Sr_2RuO_4. Fitting $C_p = \gamma T + \beta T^3$ to each trace between 1.5 and 7 K gives $\gamma = 38.2\,\mathrm{mJ/Rh\,mol\,K^2}$ for Sr_2RuO_4, in good agreement with published results. For Sr_2RhO_4 the corresponding values are $\gamma = 17.7 \pm 0.5\,\mathrm{mJ/Rh\,mol\,K^2}$ and $\beta = 0.155\,\mathrm{mJ/Rh\,mol\,K^4}$ respectively. The phononic contribution corresponds to a Debye temperature in Sr_2RhO_4 of approximately 440 K.

dominated by the Pauli term, although we have not yet performed any analysis taking into account the van Vleck contribution. At low temperatures, a Curie-like tail is seen, which is particularly pronounced for $B\|c$. Further measurments are in progress to determine whether this is intrinsic, or due to the presence of impurity spins. Its existence leaves open the question of whether there may be a link to the unusual resistivity exponent mentioned above.

2.5. Kadowaki–Woods and Wilson ratios

It is conventional when reporting the properties of new correlated electron metals to 'benchmark' them in the field by estimating and quoting two widely used characteristic ratios. The first of these, the Kadowaki–Woods ratio, compares the square of the electronic specific heat coefficient with the strength of the quadratic term in the resistivity (A in $\rho = \rho_o + AT^2$). A ratio comparing the square of a scalar quantity with some component of a tensor can hardly be regarded as rigorous, but its value has been shown to differ considerably between narrow-band and conventional metals. In layered compounds, the in-plane component of the resistivity tensor is used for the comparison. In the case of Sr_2RhO_4 its estimation is even less satisfactory than usual, because the quadratic resistivity is only observed above 50 K, but using data for $50 < T < 250$ K yields $A = (3.5 \pm 0.5) \times 10^{-3}\,\mu\Omega\,\mathrm{cm\,K^{-2}}$ and a Kadowaki–Woods ratio $a_o = 1.1 \pm 0.2$. This value is fully consistent with Sr_2RhO_4 being regarded as a strongly correlated metal.

In order to characterize the magnetic properties in terms of a Wilson ratio, we adopt the unproven assumption that the low temperature magnetic susceptibility is extrinsic in origin, and

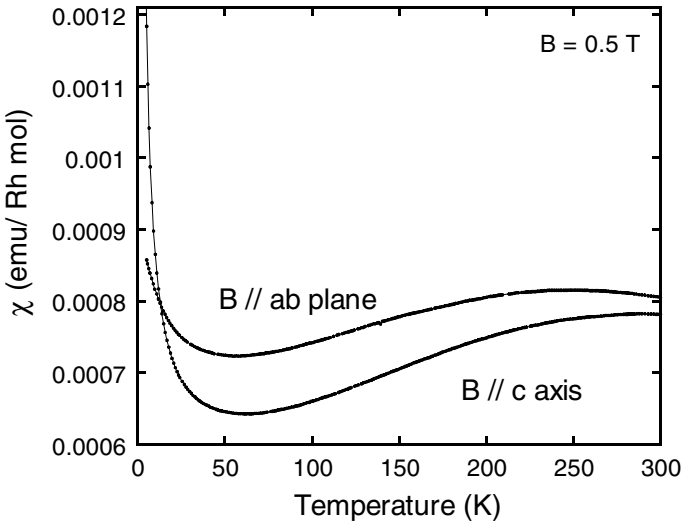

Figure 4. Raw magnetic susceptiblity (χ) of a single crystal of Sr_2RhO_4. The average value at, for example, 200 K is approximately 85% of that seen per Ru mol in Sr_2RuO_4.

subtract a Curie-like $1/T$ term from the raw data. The resulting 'intrinsic' value of χ_0 (averaged over the two orientations of applied field) is then 5.5 ± 0.5 emu/mol Rh. The Wilson ratio, R_W, is then defined in the standard way as $7.3 \times 10^4\ \chi(\text{emu/Rh mol})/\gamma\ (\text{mJ/Rh mol K}^2)$, yielding $R_W = 2.3 \pm 0.3$.

3. Spectroscopic studies

The bulk properties that we describe above have intrinsic interest because the discovery of a layered correlated oxide metal that can be purified to the extent that we describe is rare. However, the true potential of Sr_2RhO_4 to advance understanding in the field comes because of the combination of spectroscopic studies that it has been possible to perform on our single crystals. It turns out that the material cleaves very cleanly, presenting an excellent surface for the study of angle-resolved photoelectron spectroscopy (ARPES), and that the programme of purification has been sufficiently successful to allow the observation of a comprehensive and complementary set of quantum oscillation data. Parts of each of these studies have been submitted for publication elsewhere [18, 19]; in this paper we present further unpublished aspects of the projects.

3.1. ARPES

The ARPES experiments that we report were performed at Stanford in a chamber equipped with a monochromatized and modified Gammadata VUV5000 He-discharge lamp and a Scienta SES 2002 analyzer. An optimized differential pumping setup reduced the He-load in the measurement chamber to a level near the sensitivity limit of standard UHV ion-gauges. All data were taken at a temperature of 10 K and a pressure $< 4 \times 10^{-11}$ torr.

In figure 5(a), we show a photoemission Fermi surface map combining data with two different excitation energies that cover an extended momentum space range. For both energies,

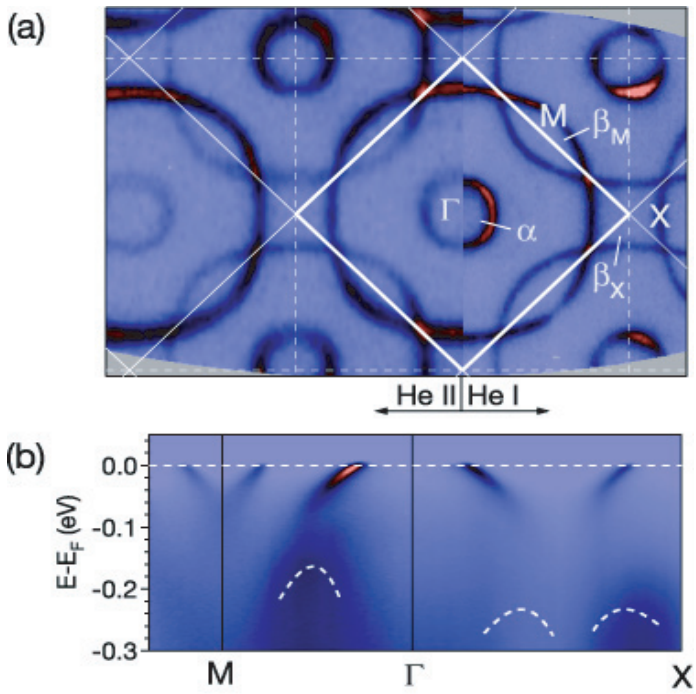

Figure 5. Photoemission quasiparticle Fermi surface and band structure of Sr_2RhO_4. (a) Fermi surface map covering multiple Brillouin zones. Data in the left and right half are taken with He IIα (40.8 eV) and He Iα (21.22 eV) radiation using effective energy resolutions of 23 and 9 meV, respectively. (b) Dispersion plot along the MΓX line of the surface Brillouin zone. The dashed white lines indicate the extrema of the d_{xy} band from an LDA calculation that has been scaled and shifted in energy.

full spectra have been measured for more than 10^4 emission angles by rotating the sample with a computer controlled cryogenic goniometer. Typically 400 sample orientations are measured and for each orientation 40 spectra covering an angular window of $\pm 6^\circ$ are acquired in parallel. Note that the data have not been symmetrized or translated. Only the directly measured momentum space is shown. A full data set contains more than 200 k-space maps at energy intervals of 1 meV. The supplementary animation file shows a sequence of these maps in the form of a movie.

Figure 5(b) depicts the energy dependence in a more conventional way as a dispersion plot. The well-defined quasiparticle bands constituting the Fermi surface are readily identified and allow a straight-forward assignment of the carrier polarity in all three Fermi surface pockets. The central α-pocket as well as the square-shaped pocket at the X-point (β_X) are hole-like with averaged Fermi velocities of 0.41(4) eV Å (6.2(6) 10^4 ms^{-1}) and 0.55(6) eV Å, (8.4(9) 10^4 ms^{-1}) respectively, while the lens-shaped pocket (β_M) is electron-like with v_F = 0.61(6) eV Å (9.3(9) 10^4 ms^{-1}). We have shown previously [18] that the volumes as well as the cyclotron masses of all three pockets deduced from the ARPES data are in quantitative agreement (within the experimental accuracy of ARPES) with the bulk specific heat and the quantum oscillation data presented below and in [19].

The most surprising feature of the Sr_2RhO_4 Fermi surface is the absence of the in-plane Rh-d_{xy} derived band. In the undistorted tetragonal zone (dashed lines in figure 5(a)), only two

bands are observed, a large electron-like pocket with a Fermi wave vector k_F of $\approx 0.66\,\text{Å}^{-1}$ and a smaller hole pocket with $k_F \approx 0.17\,\text{Å}^{-1}$. The number and size as well as the rounded-square shape of these Fermi surface contours indicates that they derive from the Rh $d_{xz,yz}$ orbitals and correspond to the α, β pockets of Sr_2RuO_4. The notion of a fully occupied d_{xy} orbital is further supported by the Luttinger volume of 3.006(10) electrons/Rh deduced from the quantitative analysis of the data in figure 5(a) [18].

Naively, one might expect to describe the Fermi surface of Sr_2RhO_4 by rigidly shifting the well-characterized band structure of Sr_2RuO_4 to accommodate the extra electron of the Rh^{4+} ion. A tight-binding calculation shows that this would reverse the character of the γ-pocket in Sr_2RuO_4 from electron- to hole-like, but would not remove it from the Fermi surface [21]. Experimentally, it is very important first to determine beyond any reasonable doubt that there is no contribution to the Fermi surface from a small d_{xy}-based sheet. The only conceivable doubt about this point in relation to the data shown in figure 5 is due to the possibility (discussed in subsection 2.1) of slight hole doping in the crystals. Strictly speaking, this means that the Luttinger volume might not correspond to integer filling. Assuming a maximum non-stoichiometry of 0.1 excess oxygens per formula unit could lead to a hole doping of as much as 0.2 per Rh. If, playing devil's advocate, one postulates that the ARPES-observed α sheet might consist of *two* almost perfectly overlapping sheets, one of which results from the d_{xy}-based band, the resulting prediction for the Luttinger count would still lie within the range allowed by this level of hole doping. Although it seems highly implausible that two bands could overlap this closely without some ARPES-observable splitting, it cannot be absolutely ruled out on the basis of ARPES data in isolation. We believe, however, that we can indeed rule it out by combining the ARPES information with that deduced from quantum oscillations as described in the next subsection.

3.2. Observation of quantum oscillations in Sr_2RhO_4

Quantum oscillations are a consequence of Landau quantization of quasiparticle orbits in a strong magnetic field leading to an oscillation, periodic in reciprocal field, of the free energy and the density of states at the Fermi level. This in turn causes oscillations in most of the physical properties, with the best known observable consequences occurring in the magnetization (the dHvA effect) or the magnetoresistance (the Shubnikov–de Haas effect) [20]–[22]. The experimental signal is extremely strongly damped by impurity scattering and is unobservable in the vast majority of oxide metals. In our early crystals of Sr_2RhO_4, searches for quantum oscillations were unsuccessful, but we finally performed a series of successful experiments. Data from the first of these, a torque magnetization study performed at the US National High Magnetic Field Laboratory in Tallahassee, are shown in figure 6.

Once quantum oscillations have been observed, they yield topographical information through a simple relationship between their frequencies and extremal Fermi surface areas in the plane perpendicular to the applied magnetic field, information on the quasiparticle density of states or 'effective mass' through analysis of the temperature dependence of their amplitudes and information on the quasiparticle mean free path through analysis of the dependence of their amplitude on magnetic field. In principle, high accuracy information can be obtained both for the extremal areas (typically 1%, corresponding to $\approx 10^{-3}$ electrons/FS pocket in Sr_2RhO_4) and effective masses (typically 2–5%), so that if the entire Fermi surface has been observed in a quasi-two-dimensional material, it should be possible to use quantum oscillation data to calculate the electronic specific heat coefficient γ to an accuracy of better than 5%.

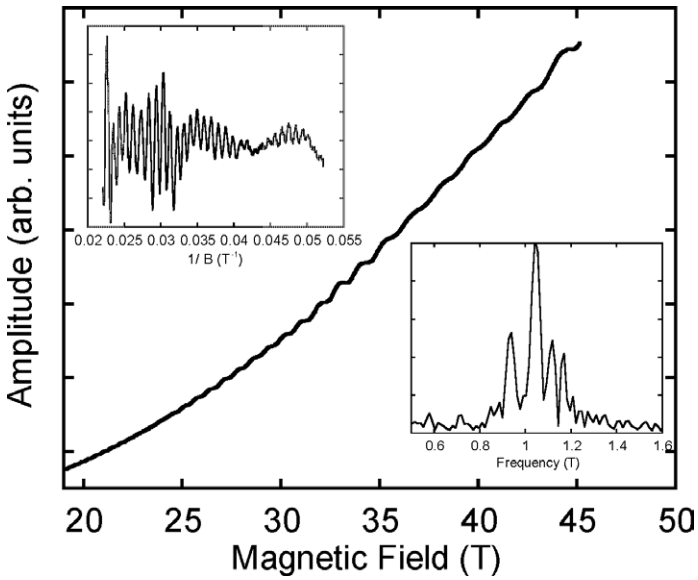

Figure 6. Magnetic torque data from a capacitive torque magnetometer operating in a plastic dilution refrigerator in the 45 T steady field magnet at the US National High Magnetic Field Laboratory, Tallahassee. The main figure shows raw data between 20 and 45 T, with the oscillatory component becoming visible above approximately 25 T. The top inset shows the result of subtracting the smooth background using a 6th order polynomial and plotting the resultant data as a function of reciprocal field. The Fourier transformation of these data is shown in the bottom inset, with four frequency components clearly visible. The temperature is 0.5 K and the magnetic field is aligned 8° from the crystallographic *c*-axis.

The fact that four peaks are seen in the Fourier transform in the lower inset to figure 6 does not mean that the quantum oscillations are resolving four distinct Fermi surfaces. The high precision of the frequency measurement compared to the 'area resolution' of ARPES (typically $\approx 10^{-2}$ electrons/FS pocket) means that extra features due to *c*-axis warping of a quasi-two-dimensional Fermi surface can also be resolved. In fact, using even higher resolution Shubnikov–de Haas measurements reported elsewhere we were able to resolve a total of seven distinct frequencies [19]. This is an unusual situation for a dHvA study— the peak splitting due to warping effects on individual Fermi surface sheets is of the same order as the area differences from one sheet to another. The challenge was to measure each of the quasiparticle masses with high precision, to investigate whether a model based on three distinct Fermi surfaces (as suggested by the ARPES work) or four matched the bulk specific heat better. In order to perform the analysis, careful account had to be taken of an effect that we have not previously seen described in the quantum oscillation literature.

3.3. Subtleties with high precision mass analysis in dHvA

To perform a mass analysis in dHvA, one plots the temperature dependence of the amplitude of the frequency concerned, and then fits the Fermi liquid Lifshitz–Kosevich (LK) formula to the data. The relevant formula, discussed in all the standard texts on dHvA, can be summarized here

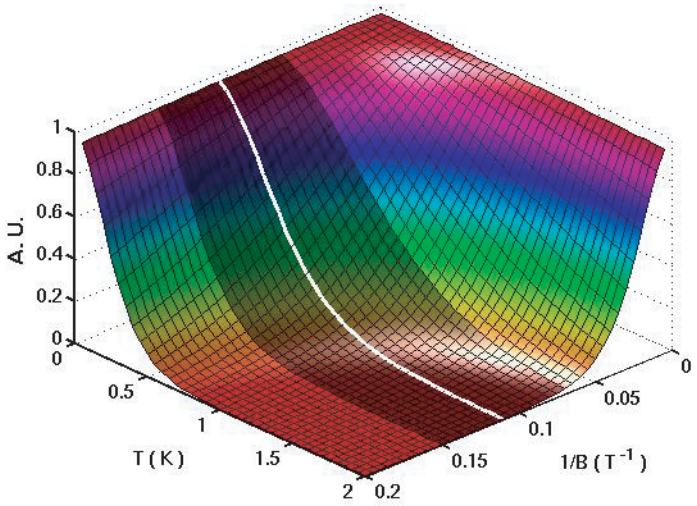

Figure 7. Surface plot of the LK formula as a function of temperature T and inverse magnetic field $1/B$. The shaded region refers to an example data analysis where data between 6 and 15 T would be put in the FFT routine and then fitted to the LK function, using an average magnetic field of 9.1 T. The white solid line refers to the LK function at the average field of 9.1 T. It can be easily seen that the LK function varies significantly over that region as function of inverse field. Numerical calculations show that in this specific case, the result is that the effective electron mass calculated using the standard central reciprocal field approximation (see text) is 25% smaller than the real value.

as the product $R_T R_D$, where

$$R_T = \frac{X}{\sinh X} \qquad X = \frac{2\pi^2 p k_B T}{\hbar \omega_c} = \frac{2\pi^2 p m^* k_B T}{e\hbar B}, \qquad R_D = \exp\left(\frac{-2\pi^2 p m^* k_B T_D}{e\hbar B}\right)$$

In these formulae T is temperature, m^* is the quasiparticle effective mass, p is the harmonic number of the oscillation concerned (usually 1), B the applied magnetic field, and $\hbar$, k_B and e Planck's constant, Boltzmann's constant and the electronic charge respectively. The Dingle temperature T_D is an effective temperature associated with elastic scattering from impurities.

Strictly speaking, observed amplitude of the peak is given by the product $R_T R_D E$, where E is an envelope function determined by the windowing used in performing the Fourier transform, the experimental conditions of measurement and, for example, the existence of beats in the data due to a multi-component signal such as that shown in the upper inset to figure 6. The approximation that is normally made when fitting its temperature dependence is that the field range over which the signal is Fourier transformed is small enough that it can be assumed to be represented by a single 'central' field, usually chosen to be the average reciprocal field of the window concerned. In fact, however, R_T, R_D and E are often highly nonlinear in field, and this can be a dangerous assumption. To illustrate this point for R_T, we plot it as a function of T and B in figure 7. The data analysis usually involves integrating over a finite width strip across the surface shown there, while the standard assumption involves using a line at constant field.

In Sr_2RhO_4 this problem was quite acute because in order to split the peaks in the transform and study their masses individually, a broad field range had to be used. To correct for this, we

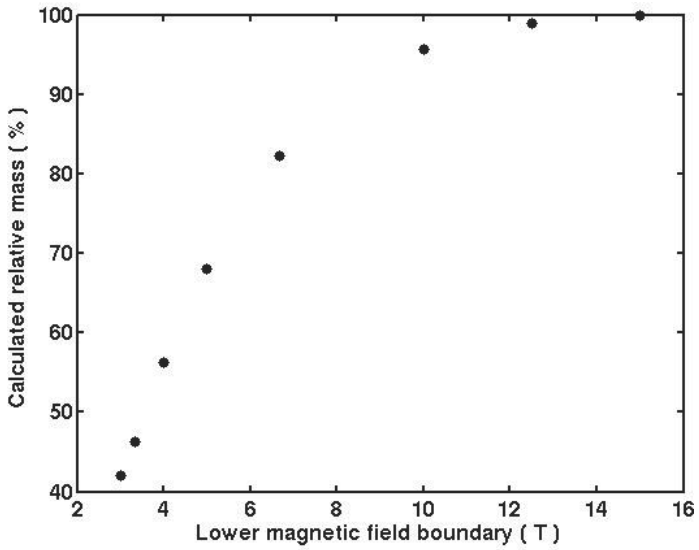

Figure 8. Fraction of the true effective electron mass extracted from a fit of simulated data to R_T using the central reciprocal field approximation. The upper boundary on the data is kept fixed at 15 T, and the result of the fit is plotted as a function of the lower boundary of the fitted data set (black dots). The effective electron mass and Dingle temperature used in the simulation were, respectively, $3m_e$ and 1.5 K. One can see that the effective electron mass is always underestimated, and that the error can be more than 50% if the central field assumption is applied to a particularly wide field range.

modelled the consequences numerically, producing results such as those depicted in figure 8. There, we simulate data with a frequency of $1\,kT$ and mass $m^* = 3m_e$ typical for Sr_2RhO_4, and plot the mass that one obtains using the 'central reciprocal field' approximation applied to transforms taken from data with variable field windows. Back correction could then be applied to the real analyses using a self-consistent procedure. The results of doing this are reported and discussed in detail in [19] and provide strong evidence that the model of three distinct FS sheets deduced from first examination of the ARPES data is correct. If four sheets are assumed, the calculation of the electronic specific heat is 20% higher than the measurement shown in figure 3, a discrepancy that is well outside our estimate of experimental error.

4. Discussion

The results that we have presented here and in [18, 19] give strong evidence that the naïve picture that the electronic structure of Sr_2RhO_4 can be well approximated by a rigid band shift placing an extra electron into the band structure of Sr_2RuO_4 is incorrect. The reason for this is probably that it ignores a structural distortion in the rhodate. The rotation of the RhO_6 octahedra around the c-axis by 11° has a profound influence on the band structure. It does not significantly modify the $d_{xz,yz}$ derived bands, since hopping between these orbitals occurs mainly through the rotationally symmetric O $2p_z$, but it strongly couples to the in-plane d_{xy} orbital. Moreover, the distortion reduces the symmetry and thus allows hybridization of the d_{xy} orbital with a wide band derived from e_g $d_{x^2-y^2}$ states. LDA calculations indicate that this hybridization is strong enough

to produce an absolute band gap in the unoccupied states and push the d_{xy} band just below the Fermi level [23, 24]. If this picture applies, one would expect additional features in the dispersion plot of figure 5(b) that cannot be assigned to the α and β pockets. The calculations predict that the top of the d_{xy} band lies less than 10 meV below the Fermi level half way between Γ and M. Two additional extrema are calculated at -0.19 eV near 0.4 ΓX and 0.8 ΓX. Around the predicted top of the band in the immediate vicinity of the Fermi level, one expects to see sharp and well-defined quasiparticle peaks, comparable to those observed for the α and β pockets. Clearly, such a band is not observed in the data. However, at two of the three predicted locations, we find signatures at lower energy. The clearest one lies at -0.17 eV between Γ and M and may correspond to the predicted top of the d_{xy} band. This state is already severely broadened, consistent with the increased phase space for electron–electron scattering at these energies. An even broader feature can be discerned at -0.27 eV near 0.85 ΓX.

We have shown previously that the LDA calculation for Sr_2RhO_4 captures the essential topology of the lowest lying excitations, but finds relative positions of the relevant bands that are significantly different from the experiment [18]. This inaccuracy may be related to the inability of the local density approximation to properly account for local correlations. However, it mainly affects energy positions of the bands. The momenta of extremal points in the band structure are more robust. Indeed if the LDA calculation is renormalized in energy by a factor of two to account in first order for a Fermi-liquid like self-energy and shifted down by 0.16 eV (dashed white lines in figure 5(b)), the d_{xy} related features appear to match the experimental data. This would be consistent with the basic one-electron picture that structural distortions remove the d_{xy} orbital from the Fermi surface of Sr_2RhO_4, but at the same time highlights the inability of the LDA to properly account for the energetics in this correlated metal.

A further interesting point is that the combination of spectroscopies that we have been able to apply to Sr_2RhO_4 has led to a conclusion that is relevant to our understanding of its chemistry. Once the existence of only three Fermi surface sheets is established, the Luttinger count from either our ARPES (subsection 3.1) or quantum oscillations [19] is consistent, within experimental error of 1%, with an integer number of three conduction electrons per Rh. This in turn provides quite strong evidence that the oxygen uptake seen in our thermogravimetric analysis (subsection 2.1) takes the crystals from oxygen deficiency towards stoichiometry rather than introducing an oxygen excess. This hypothesis should be checked in future using other techniques such as neutron scattering.

Finally, we stress that although the observation of a resistivity exponent of 2.4 at low temperatures remains somewhat mysterious, all the quantum oscillation and ARPES data that we have gathered so far have been fully consistent with the metallic state of Sr_2RhO_4 being a Fermi liquid. More work is planned to investigate the origin of this unusual transport behaviour.

5. Summary

In this paper we have reported the details of a long project to grow and purify single crystals of a new strongly correlated electron oxide, Sr_2RhO_4. After careful annealing, residual resistivity ratio in excess of 100 have been achieved, enabling the observation of both the Shubnikov-de Haas and dHvA effects in the best crystals. An added bonus is favourable cleaving properties which have also allowed us to perform high resolution angle-resolved photoemission studies on the same crystals. The combination of information that we have gathered has established Sr_2RhO_4 as a 'benchmark' high purity correlated electron metal.

Acknowledgments

The authors would like to thank J Farrell, S A Grigera, R Borzi, W Meevasana, R Dunkel, K M Shen, D H Lu, K Kamenev, J P Attfield, J Irvine and T P Murphy for helpful discussions and technical assistance. We also thank B J Kim and C Y Kim for discussion and for provision of [23] prior to publication. We performed the measurements of C_p at the University of Edinburgh under an equipment sharing arrangement as part of the Scottish Universities Physics Alliance. This work has been supported by the Engineering and Physical Sciences Research Council Portfolio Partnership 'Novel Quantum Order in Interacting Electron Metals', the Leverhulme Trust, and ONR grant N00014-01-1-0048. Additional support from SSRL was provided by the DOE's office of Basic Energy Science, Division of Material Science with contract DE-FG03-OIER45929-A001.

References

[1] Damascelli A, Hussain Z and Shen Z X 2003 *Rev. Mod. Phys.* **75** 473–541
[2] Tokura Y and Nagaosa N 2000 *Science* **288** 462
[3] Stewart G R 2001 *Rev. Mod. Phys.* **73** 797–855
[4] Nakatsuji S and Maeno Y 2000 *Phys. Rev. Lett.* **84** 2666
[5] Mackenzie A P and Maeno Y 2003 *Rev. Mod. Phys.* **75** 657–712
[6] Grigera S A *et al* 2004 *Science* **306** 1155
[7] Allen P B, Berger H, Chauvet O, Forro L, Jarlborg T, Junod A, Revaz B and Santi G 1996 *Phys. Rev.* B **53** 4393
[8] Mackenzie A P, Reiner J W, Tyler A W, Galvin L M, Julian S R, Beasley M R, Geballe T H and Kapitulnik A 1998 *Phys. Rev.* B **58** R13318
[9] Ikeda S, Maeno Y, Nakatsuji S, Kosaka M and Uwatoko Y 2000 *Phys. Rev.* B **62** R6089
[10] Mao Z Q, Zhou M, Hooper J, Golub V and O'Connor C J 2006 *Phys. Rev. Lett.* **96** 077205
[11] Baumberger F *et al* 2006 *Phys. Rev. Lett.* **96** 107601
[12] Mao Z Q, Maeno Y and Fukazawa H 2000 *Mater. Res. Bull.* **35** 1813
[13] Perry R S and Maeno Y 2004 *J. Cryst. Growth* **271** 134
[14] Varela A, Boulahya K, Parras M, Gonzales-Calbet J M, Vogt T and Buttrey D J 2001 *Chem.— Eur. J.* **7** 1444
[15] Mackenzie A P, Haselwimmer R K W, Tyler A W, Lonzarich G G, Mori Y, Nishizaki S and Maeno Y 1998 *Phys. Rev. Lett.* **80** 161
[16] Capogna L *et al* 2002 *Phys. Rev. Lett.* **88** 076602
[17] Maeno Y *et al* 1997 *J. Phys. Soc. Japan* **66** 1405
[18] Baumberger F, Ingle N J C, Meevasana W, Shen K M, Lu D H, Perry R S, Mackenzie A P, Hussain Z, Singh D J and Shen Z-X 2006 *Phys. Rev. Lett.* **96** 246402
[19] Perry R S, Kikugawa N, Balicas L, Rost A, Mercure J F, Maeno Y and Mackenzie A P 2006 *Phys. Rev. Lett.* submitted
[20] Shoenberg D 1984 *Magnetic Oscillations in Metals* (Cambridge: Cambridge University Press)
[21] Bergemann C, Mackenzie A P, Julian S R, Forsythe D and Ohmichi E 2003 *Adv. Phys.* **52** 639–725
[22] Bergemann C 2005 Fermi surface measurements *Encyclopedia of Condensed Matter Physics* ed G Bassani (London: Elsevier)
[23] Kim B J *et al* 2006 *Phys. Rev. Lett.* submitted
[24] Singh D J 2006 private communication